

See discussions, stats, and author profiles for this publication at: <https://www.researchgate.net/publication/273381960>

An Analytical Unit Cell Model for the Effective Thermal Conductivity of High Porosity Open-Cell Metal Foams

Article in *Transport in Porous Media* · February 2014

DOI: 10.1007/s11242-014-0281-z

CITATIONS

12

READS

81

6 authors, including:



[Xiaohu Yang](#)

Xi'an Jiaotong University

30 PUBLICATIONS 101 CITATIONS

[SEE PROFILE](#)



[Hongbin Yan](#)

Northwestern Polytechnical University

10 PUBLICATIONS 31 CITATIONS

[SEE PROFILE](#)



[Tian Jian Lu](#)

Xi'an Jiaotong University

551 PUBLICATIONS 8,635 CITATIONS

[SEE PROFILE](#)

Some of the authors of this publication are also working on these related projects:



metallic glasses [View project](#)



Enhancement of upconversion [View project](#)

An Analytical Unit Cell Model for the Effective Thermal Conductivity of High Porosity Open-Cell Metal Foams

Xiao Hu Yang · Jia Xi Bai · Hong Bin Yan ·
Jiu Jie Kuang · Tian Jian Lu · Tongbeum Kim

Received: 3 November 2013 / Accepted: 15 January 2014 / Published online: 1 February 2014
© Springer Science+Business Media Dordrecht 2014

Abstract We present an analytical model for the effective thermal conductivity of fluid-saturated metal foams with open cells. For high porosity ranges ($\varepsilon \geq 0.9$), the model is derived based on a realistic representative unit cell (a tetrakaidecahedron with cuboid node) under the assumption of parallel heat conduction along the highly tortuous cell ligaments and the saturating fluid. Good agreement with existing experimental data as well as the present measurements of open-cell aluminum foams saturated with either air or water validates the present model. More realistic and reasonable node size is estimated and compared with other model predictions. Ligament shape and pore size (PPI) are found to have little influence upon the effective thermal conductivity of the bulk porous media. Further, the influence of the fluid phase as well as the interactive heat conduction between solid and fluid phase on the overall effective thermal conductivity is quantified.

Keywords Effective thermal conductivity · Porous media · Unit cell modeling · Node size · Heat conduction

X. H. Yang (✉) · H. B. Yan · J. J. Kuang
School of Energy and Power Engineering, Xi'an Jiaotong University,
Xi'an 710049, People's Republic of China
e-mail: thomasyangfly@126.com

J. X. Bai · T. J. Lu (✉)
State Key Laboratory for Strength and Vibration of Mechanical Structures,
School of Aerospace, Xi'an Jiaotong University, Xi'an 710049, People's Republic of China
e-mail: tjlu@mail.xjtu.edu.cn

T. Kim (✉)
School of Mechanical Engineering, University of the Witwatersrand,
Johannesburg, Wits 2050, South Africa
e-mail: tongkim@wits.ac.za

List of Symbols

Variables

A_0	Heat transfer area of control volume (m^2)
A_L	Cross-sectional area of ligament (m^2)
$A_L(s)$	Cross-sectional area of ligament along solid ligaments (m^2)
A_f	Heat transfer area of fluid phase in control volume (m^2)
A_t	Cross-sectional area of node (m^2)
a	Thickness of solid ligament (m)
e	Thickness ratio of node to solid ligament, $e = t/L$
H_c	Height of control volume (m)
$H(s)$	Vertical height of control volume along ligament (m)
k_e	Effective thermal conductivity of porous media (W/m K)
k_s	Thermal conductivity of solid ligament (W/m K)
k_f	Thermal conductivity of saturating fluid (W/m K)
L	Length of solid ligament (m)
Q_t	Total heat transported through control volume (W)
Q_s	Heat transported through solid ligaments in control volume (W)
Q_f	Heat transported through saturating fluid in control volume (W)
s	Axis along solid ligament
t	Thickness of cuboid node (m)
V_L	Volume of the ligaments in control volume (m^3)
V_t	Volume of the nodes in control volume (m^3)
V_{CV}	Volume of control volume (m^3)

Greek Symbols

α	Cross-sectional area ratio of cuboid node to ligament
ε	Porosity
ρ^*	Relative density, $\rho^* = 1 - \varepsilon$
φ	Ratio of ligament cross-sectional area at ends to that at center

1 Introduction

With ultra low density, high surface area to volume ratio, relatively low cost, and especially fluid mixing ability, high porosity open-cell metallic foams (Fig. 1a) are attractive for a variety of unique thermal-fluidic applications such as microelectronics cooling (Lu et al. 1998), fuel cells (Kumar and Reddy 2003; Tawfik et al. 2007), and compact heat exchangers (Lu et al. 1998; Hunt and Tien 1988; Tawfik et al. 2007; Tadrist et al. 2004; Haack et al. 2001). Open-cell aluminum (Al) and copper foams are the most widely applied metallic foams for thermal management applications. For optimal design and analysis of thermal management systems involving metallic foams, evaluating the effective thermophysical properties of the foam, e.g., effective thermal conductivity, plays a pivotal role (Lu et al. 1998; Hunt and Tien 1988).

Open-cell metallic foams have porous cellular structure consisting of inner-connected pores and fiber-made skeleton. To model the effective thermal conductivity, a precise description of foam topology is essential for the analysis on thermal transport in the foam. Predictions

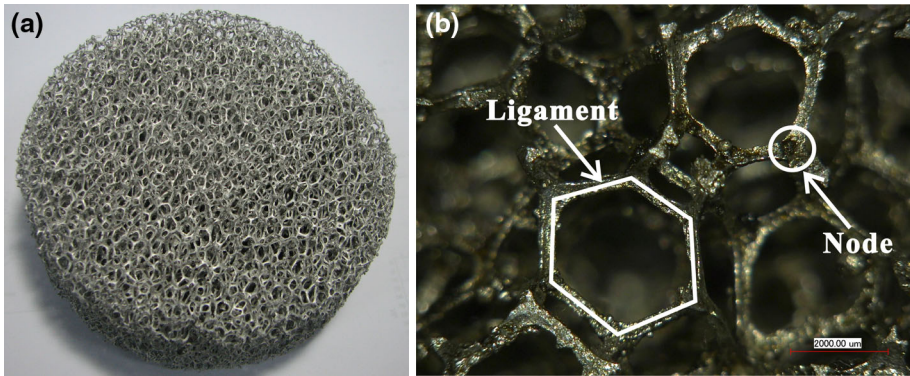


Fig. 1 **a** High porosity aluminum (Al) foam with open cells ($\epsilon = 0.92$); **b** scanning electronic microscope (SEM) image of Al foam

using classical analytical models ([Maxwell 1881](#); [Progelhof et al. 1976](#); [Tsotsas and Martin 1987](#)) are less accurate due to idealized assumptions such as: (i) series or parallel configuration of solid and fluid phases; (ii) random distribution of each phase ([Landauer 1952](#); [Russell 1935](#)), (iii) symmetrical distribution of solid and fluid phases ([Hsu et al. 1994](#)). Subsequently, focusing upon open-cell Al foams saturated in a fluid phase, [Calmidi and Mahajan \(1999\)](#) proposed a two-dimensional (2D) unit cell having a hexagonal honeycomb shape with square nodes at each joint, as illustrated in Fig. 1b. However, through best fit to experimental data ([Calmidi and Mahajan 1999](#)), the node size t/a (ratio of node thickness to half of ligament thickness) was found to be unrealistically large (22.22). [Bhattacharya et al. \(2002\)](#) replaced the square node by circular node and found that the node size was considerably reduced, from 22.22 to 10.53, but still large. The prediction of large node sizes by these models may be attributed to the idealized 2D topology representation of the three-dimensional (3D) open-cell Al foam shown in Fig. 1a.

Adopting a 3D tetrakaidecahedron unit cell with cubic nodes at each joint to represent the topology of metallic foams, [Boomsma and Poulikakos \(2001\)](#) put forward an important and widely referred to model for the effective conductivity of metallic foams. However, after a careful review, [Dai et al. \(2010\)](#) revealed that the Boomsma–Poulikakos model “contains errors in its development and presentation. Whether partially or fully corrected, the model does not provide accurate predictions of the effective thermal conductivity of metal foams.” By accounting for ligaments orientation, [Dai et al. \(2010\)](#) corrected and modified the original Boomsma–Poulikakos model, achieving better agreement with experimental data. Nevertheless, neither the original nor modified Boomsma–Poulikakos model gives reasonable estimate of the node size for open-cell metallic foams: shrunken nodes at relatively low porosities ($0.90 < \epsilon < 0.97$) and expanded nodes at relatively high porosities ($\epsilon > 0.97$), both deviating from the real foam structure.

An accurate representation of the open-cell metallic foam morphology is of significance not only for predicting the effective thermal conductivity but also for providing the physical basis as well as insight into the transport phenomena in porous media. This study aims to squarely address the deficiency of node prediction by existing models and achieve reasonable estimate of node size by developing an analytical model for the effective thermal conductivity of open-cell metallic foams. To this end, heat conduction in a 3D tetrakaidecahedron unit cell is considered, assuming one-dimensional (1D) conduction along highly tortuous-conducting ligaments with cuboid nodes and parallel conduction through the saturating fluid phase (air

or water). For model validation, experimental measurements of node size as well as effective thermal conductivity for air or water-saturated Al foam samples are performed.

2 Analytical Model Developments

2.1 Description of Open-Cell Metal Foam Topology

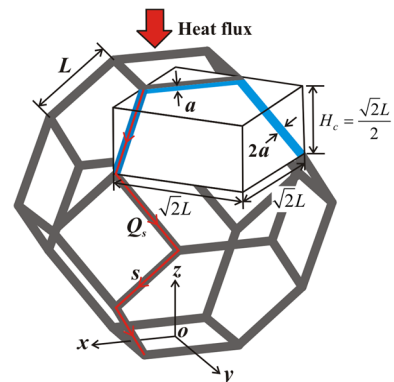
Open-cell Al foams are typically fabricated by direct foaming, seepage casting and precision casting. Amongst these fabrication methods, precision casting is capable of providing relatively high porosity Al foams having uniform pore size, cellular structure and good 3D connectivity which other methods do not possess. The method of precision casting requires a precast porous gypsum block, which is commonly prepared by volatilizing polyester sponge foams saturated with gypsum slurry through heat treatment. Aluminum melt is then infiltrated into the gypsum block. After the melt is solidified and the gypsum removed, metallic foams having the same topology as the polyester sponge foam can be precisely made.

Polyester sponge foams are fabricated via direct foaming, during which the foaming gas in the molten slurry moves freely, forming eventually tetrakaidecahedron cells to maintain minimal surface energy (Thompson 1942; Thomson 1887; Weaire and Hutzler 1999). As shown in Fig. 1b, there exists nodes where the ligaments join each other and most of the joints are *slightly* thicker than the ligaments. To simplify the present analysis, Al foams fabricated via precision casting may therefore be considered to have the topology of periodically distributed tetrakaidecahedron cells. Each tetrakaidecahedron is consisted of six squares and eight hexagonal faces having a uniform ligament length and thickness with cuboid nodes, as illustrated in Fig. 2.

2.2 Analytical Expression Assuming One-Dimensional Heat Conduction

For a tetrakaidecahedron unit cell fully saturated in a fluid phase as depicted in Fig. 2, let k_e denote its effective thermal conductivity and let k_s and k_f denote the thermal conductivity of the solid ligament material and the saturated fluid phase. Due to symmetry, we only consider one-sixteenth out of a single tetrakaidecahedron cell as a control volume (CV), namely, a cuboid with the dimension of $\sqrt{2}L$ (length) \times $\sqrt{2}L$ (width) \times $\sqrt{2}L/2$ (height); see Fig. 2. This CV contains two entire ligaments each with length L and thickness $2a$ as well as a partial

Fig. 2 Open-cell Al foams modeled with a tetrakaidecahedron unit cell consisted of square cross-sectioned ligaments with uniform thickness $2a$ and length L . The *cuboid* denotes a control volume (CV) for one-sixteenth of a single tetrakaidecahedron unit cell



ligament having L in length and a in thickness. Following Fourier’s law of heat conduction, the total amount of heat transferred through the CV may be expressed as:

$$Q_t = k_e A_0 \frac{\Delta T}{H_c}, \tag{1}$$

where A_0 is the heat transfer area of the CV, H_c is the thickness of the CV, and ΔT is the temperature difference across the CV along the z -axis.

The total amount of heat transferred to the CV is conducted along the solid ligaments (k_s) and the fluid (k_f) in parallel, i.e., $Q_t = Q_s + Q_f$ (the interactive heat conduction between saturating fluid and solid ligaments will be discussed later). By Fourier’s law, the heat conducted along the ligaments may be expressed as:

$$Q_s = -k_s A_L(s) \frac{dT}{ds}, \tag{2}$$

where s is the axis along the ligaments which is strongly dependent on the topology of the porous medium of interest, and $A_L(s)$ representing the cross-sectional area of each ligament is a function of ds independent of dT . To solve Eq. (2), the method of separation of variables is applied, yielding:

$$\frac{Q_s}{A_L(s)} ds = -k_s dT. \tag{3}$$

Integration of Eq. (3) from the top to the bottom of the CV leads to:

$$Q_s \int_0^{H(s)} \frac{1}{A_L(s)} ds = -k_s T|_0^{H_c}. \tag{4}$$

Note that the heat Q_s along the tortuous ligaments is assumed to be constant (through ligaments having identical cross-sectional area). Mathematical manipulation of Eq. (4) yields:

$$Q_s = k_s \Delta T \left/ \left(\int_0^{H(s)} \frac{1}{A_L(s)} ds \right) \right. . \tag{5}$$

For heat transferred through the saturating fluid phase in the CV, Fourier’s law dictates:

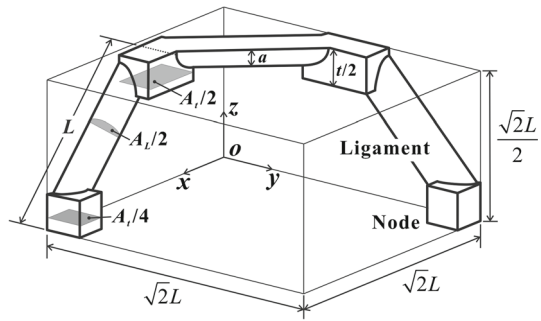
$$Q_f = k_f A_f \frac{\Delta T}{H_c}. \tag{6}$$

Finally, substitution of Eqs. (5) and (6) into Eq. (1) results in:

$$\frac{k_e}{k_s} = \left(\frac{H_c}{A_0} \right) \left/ \left(\int_0^{H(s)} \frac{1}{A_L(s)} ds \right) \right. + \frac{k_f}{k_s} \varepsilon, \tag{7}$$

where ε defines the volume fraction of the fluid phase, i.e., porosity. To analytically solve Eq. (7), the topological parameters associated with the tetrakaidecahedron need to be determined.

Fig. 3 A control volume (CV) for one-sixteenth of a single tetrakaidecahedron unit cell with cuboid nodes having thickness t and cross-sectional area A_t , the porosity is 0.958



2.3 Topological Parameters

To proceed, the node where the ligaments join as shown in Fig. 1b must be properly modeled and its size accurately determined. In reality, strongly dependent on porosity, most of the joints have relative size to the ligament thickness slightly larger than unity (Boomsma and Poulikakos 2001; Dai et al. 2010). In the present model, the nodes are regarded as cuboids having a cross-sectional area of A_t and thickness of t as illustrated in Fig. 3. Two dimensionless parameters are introduced to relate the node size (A_t, t) and the ligament size (A_L, L), as:

$$\alpha = A_t/A_L, \quad \alpha \geq 1 \tag{8a}$$

$$e = t/L, \quad e \geq 0. \tag{8b}$$

Accordingly, the relative density of open-cell foams having such tetrakaidecahedron unit cells with cuboid nodes may be obtained as (see Appendix for details):

$$\rho^* = 1 - \varepsilon = \left[\frac{6(1 - e) + 3\alpha e}{4\sqrt{2}} \right] \times \frac{A_L}{L^2}. \tag{9}$$

With reference to Fig. 3, the variation of heat transfer area integrated along the s -direction and the heat transported through solid ligaments may be separately calculated as:

$$\int_0^{H(s)} \frac{1}{A_L(s)} ds = \left(1 - e + \frac{3e}{2\alpha} \right) \frac{L}{A_L} \tag{10a}$$

$$\left(\frac{H_c}{A_0} \right) / \left(\int_0^{H(s)} \frac{1}{A_L(s)} ds \right) = \frac{\sqrt{2}}{4(1 - e + \frac{3e}{2\alpha})} \times \frac{A_L}{L^2}. \tag{10b}$$

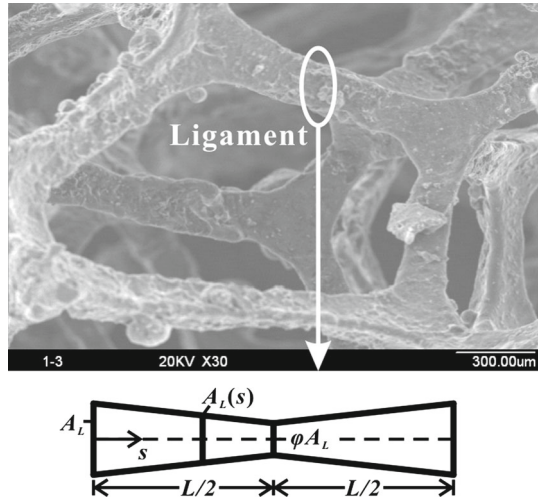
Substitution of (9) and (10b) into (7) yields the final expression for the effective thermal conductivity of open-cell metal foams, as:

$$\frac{k_e}{k_s} = \frac{(1 - \varepsilon)}{\left(1 - e + \frac{3e}{2\alpha} \right) \left[3(1 - e) + \frac{3}{2}\alpha e \right]} + \frac{k_f}{k_s} \varepsilon. \tag{11}$$

2.4 Cross-sectional Shape of Cell Ligament

The representative cellular topology of precision cast Al foams with open cells has been idealized as tetrakaidecahedron with identical and uniform ligaments. However, it needs to

Fig. 4 Cross-sectional shape of cell ligaments: from SEM image to idealized linear variation



be recognized here that, the metallic ligaments look like dumbbells, thicker at both ends but thinner in the middle (see Fig. 4). To model the influence of such variation in ligament cross-sectional area on effective thermal conductivity, an arbitrarily selected linear functional relationship for the cross-sectional area is assumed, as illustrated schematically in Fig. 4. Consequently, the ligament cross-sectional area, depicted as $A_L(s)$, varies with the coordinate position along the s -direction, as:

$$A_L(s) = \begin{cases} -2(1 - \varphi)A_L \times \frac{s}{L} + A_L, & 0 \leq s \leq \frac{L}{2} \\ 2(1 - \varphi)A_L \times \frac{s}{L} + (2\varphi - 1)A_L, & \frac{L}{2} \leq s \leq L, \end{cases} \tag{12}$$

where φ is the proportionality coefficient defined as the ratio of ligament cross-sectional area in the middle to that at the end, $\varphi = A_L(L/2)/A_L$. The variation of heat transfer area integrated along the s -direction can thence be calculated as:

$$\int_0^{H(s)} \frac{1}{A_L(s)} ds = \frac{L}{A_L} \left[\frac{3e}{2\alpha} - \frac{\ln[1 - (1 - e)(1 - \varphi)]}{(1 - \varphi)} \right]. \tag{13}$$

Similarly, the foam relative density may be expressed as:

$$\rho^* = 1 - \varepsilon = \frac{3A_L}{4\sqrt{2}L^2} [2(1 - e) - (1 - \varphi)(1 - e)^2 + \alpha e]. \tag{14}$$

Substitution of (13) and (14) into (7) leads to a relatively simple explicit expression of the effective thermal conductivity, as:

$$\frac{k_e}{k_s} = \frac{4\alpha(1 - \varphi)}{9e(1 - \varphi) - 6\alpha \ln[1 - (1 - \varphi)(1 - e)]} \cdot \frac{1 - \varepsilon}{2(1 - e) - (1 - \varphi)(1 - e)^2 + \alpha e} + \frac{k_f}{k_s} \varepsilon. \tag{15}$$

Table 1 Parameters of open-cell aluminum foam samples used for effective thermal conductivity measurements

Sample	1	2	3	4	5	6	7	8
Material conductivity (W/mK)	236							
Volume ($W \times L \times H$)	0.068 m \times 0.068 m \times 0.022 m							
Relative density (measured)	0.088	0.087	0.083	0.077	0.072	0.047	0.043	0.037
Porosity	0.912	0.913	0.917	0.923	0.928	0.953	0.957	0.963
Pore density (PPI)	7	5	10	20	10	6	8	13

The pore size PPI is defined as pores per inch

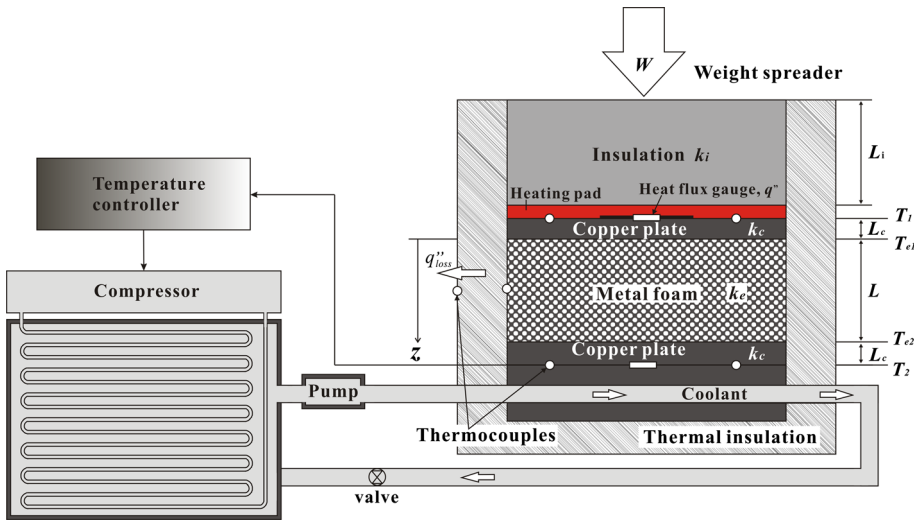


Fig. 5 Schematic of test rig for effective thermal conductivity measurements with controllable power input and thermostatic bath, with z -axis coinciding with heat-flow direction

3 Experimental Validation

3.1 Open-Cell Metal Foam Specimens

To validate the present analytical model predictions, measurements of effective thermal conductivity were carried out with 8 open-cell Al foam specimens having different pore sizes and porosities were tested, as summarized in Table 1. The specimens had the same size of 0.068 m \times 0.068 m \times 0.022 m. The material make of the foam is pure aluminum, with a thermal conductivity of 236 W/(m K). The porosity ε is obtained via the relationship $\varepsilon = 1 - \rho^*$, where ρ^* is the relative foam density.

3.2 Experimental Setup

To measure the steady-state effective thermal conductivity of open-cell Al foams saturated with air ($k_f = 0.0265$ W/m K) or water ($k_f = 0.613$ W/m K), a purposely designed test rig is built as illustrated in Fig. 5. The Al foam specimen is put into a cubic container made of a low conducting material (Perspex 0.18W/m K). The cubic container has dimensions of

0.07 m (width) × 0.07 m (length) × 0.15 m (height), with a wall thickness of 0.02 m. Two copper plates used as the substrates sandwiching the Al foam have a thermal conductivity of 398 W/(mK) (Incropera et al. 2011). A heating element attached to the outer surface of the upper copper plate is controlled by an AC power supply. To minimize heat loss, the outer surface of the container is covered with a thick thermal insulation material.

To minimize natural conduction of the fluid phase (air) fully saturating the Al foam, a constant heat flux is imposed by an etched-foil heating pad, 0.07 m × 0.07 m in size, on the upper side of the copper plate; see Fig. 5. Heat transferred via the fluid phase in the sample is therefore dominated by conduction from the top to the bottom and removed from the test cube (made of a 0.01 m thick copper plate), with coolant supplied from a cooling system (Contraves Rheotherm 115™) flowing through wound passages machined into the copper plate. To measure the temperature and net heat flux, three T-type thermocouples (Omega™) and a film-type heat flux gage are separately attached with thermal grease to the lower copper plate. To estimate the heat lost through the test section side walls, two additional T-type film thermocouples are placed on the inner and outer sides of the Perspex side wall.

The surface temperatures T_1 and T_2 are separately measured by K-type thermocouples built-in the film heat flux gage (Omega™) as well as T-type foil thermocouples (thickness 13 μm, Omega™) attached to the copper plates. As illustrated in Fig. 5, 1D heat conduction occurs along the z -axis. The effective thermal conductivity k_e of the test sample is calculated following Fourier’s steady-state heat conduction law, as:

$$k_e = -\frac{q''_{\text{net}}L}{\Delta T} \tag{16}$$

where q''_{net} is the net heat flux defined as $q''_{\text{net}} = q''_{\text{input}} - q''_{\text{loss}}$, L is the sample length along the z -axis (Fig. 5), and $\Delta T = T_{e2} - T_{e1}$ is the temperature difference between the upper and lower surfaces of the sample, estimated as:

$$T_{e2} = T_2 + \frac{q''_{\text{net}}L_c}{k_c} \tag{17a}$$

$$T_{e1} = T_1 - \frac{q''_{\text{net}}L_c}{k_c} \tag{17b}$$

Here, T_2 and T_1 are the temperatures of the lower and upper surface of the copper (substrate) plate directly measured by the attached thermocouples.

3.3 Measurement Uncertainty

Quantifying the thermal conductivity k using the present experimental setup is affected by the following parameters: q''_{net} , T_{e1} , T_{e2} , and L . With L fixed at 10 mm, the errors associated with the measurement of k_e may be estimated as (Coleman and Steele 2009):

$$\frac{\Delta k_e}{k_e} = \sqrt{\left(\frac{\Delta q''_{\text{net}}}{q''_{\text{net}}}\right)^2 + \left(\frac{\Delta T_{e1}}{T_{e1} - T_{e2}}\right)^2 + \left(\frac{\Delta T_{e2}}{T_{e1} - T_{e2}}\right)^2}, \tag{18}$$

where the error associated with the temperatures T_{e1} and T_{e2} due to film thermocouple calibration and resolution of the data acquisition device is estimated to be 0.2 °C. For the input heat flux q''_{net} measured by the film heat flux gage, the error stems mainly from signal readings by the multimeter and is estimated to be within 2.0 %. Overall, the uncertainty in the present measurement of effective thermal conductivity is estimated to be less than ±3.5 %.

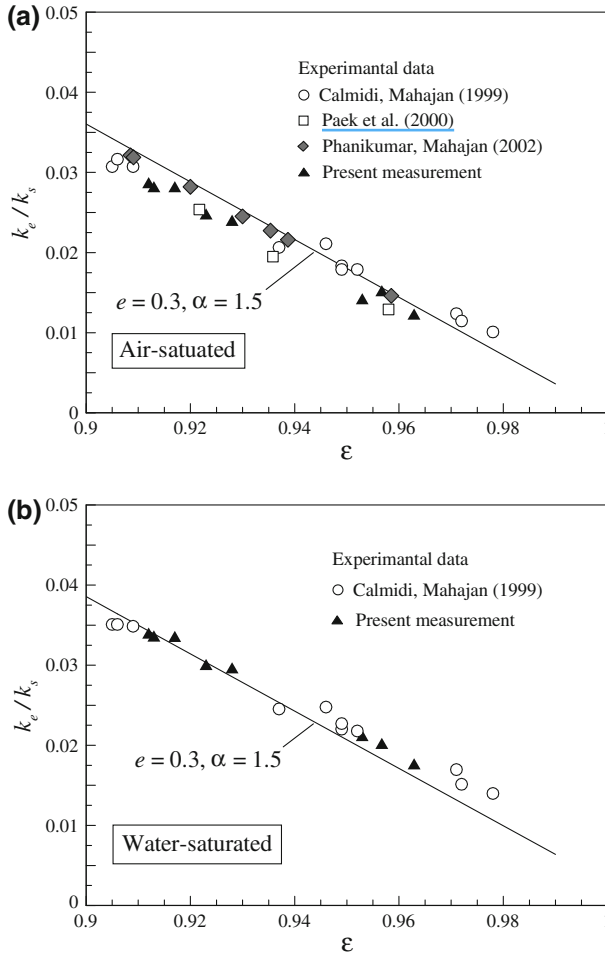


Fig. 6 Comparison of effective thermal conductivity predicted by the present model (Eq. 11) with experimental data from the present measurement and open literature (Calmidi and Mahajan 1999; Paek et al. 2000; Phanikumar and Mahajan 2002) for **a** air-saturated Al foams and **b** water-saturated Al foams having node sizes fixed at $e = 0.3$ and $\alpha = 1.5$ (see Eq. 8)

4 Results and Discussion

4.1 Dependence of Effective Thermal Conductivity on Porosity

For open-cell Al foams saturated in air or water, Fig. 6 compares the analytically predicted effective thermal conductivity using Eq. (11) with experimental data from the present measurement and open literature (Calmidi and Mahajan 1999; Paek et al. 2000; Phanikumar and Mahajan 2002). It is seen that the analytical model predicts an increasing effective thermal conductivity (k_e/k_s) with decreasing porosity in the high porosity range ($\epsilon \geq 0.9$), with node size fixed at $e = 0.3$ and $\alpha = 1.5$ (see Eq. 8). The model predicts accurately the linear variation trend of effective conductivity with porosity, where the root-mean-square (RMS) deviations from the experimental data are within 9.8 and 11.1 % for using air and water as the saturating fluid, respectively. However, a further decrease in porosity may cause the

thickening of cell ligaments for a given pore size. Heat conduction along the thickened ligaments may then violate the assumption of 1D conduction made, resulting in over-estimated effective conductivity of the foam.

For air-saturated metal foams, the thermal conductivity ratio of solid ligaments to fluid phase is typically $k_s/k_f > 8000$, so that the contribution of air to heat transfer may be neglected. With fixed node size ($e = 0.3$ and $\alpha = 1.5$), the expression of the effective conductivity simplifies to:

$$\frac{k_e}{k_s} = 0.36(1 - \varepsilon). \quad (19)$$

This prediction has a remarkably simple form - a product of the porosity and the thermal tortuosity. The proportionality coefficient 0.36 is the reciprocal of thermal tortuosity (2.78) that represents the elongated heat transfer length via tortuous thin cell ligaments (Yang et al. 2013). In open-cell metal foams especially those made of high conducting metals (e.g., pure aluminum and copper), heat is conducted essentially in parallel (i.e., via solid ligaments and saturating fluid). The negligible contribution of the fluid phase to heat conduction may be justified when the thermal conductivity ratio between the solid and fluid phases is large, e.g., $k_s/k_f > 8000$ for air-saturated Al foams.

Expect the analytical prediction of Eq. (19), there also exist empirical correlations (via test data fitting) of the effective thermal conductivity for open-cell Al foams saturated in air which have expressions similar in form to Eq. (19), with the proportionality coefficient equal to 0.35 or 0.346 (Bhattacharya et al. 2002; Ozmat et al. 2004). The present analytical model lays the physical basis of these empirical correlations in terms of (i) taking the form of the parallel model and (ii) having a similar proportionality coefficient around 0.35.

4.2 Effect of Temperature

The thermophysical properties of a substance vary with temperature. Specially, at high ambient temperatures, the effective conductivity coupling with radiative heat transfer in porous media with relatively high porosities ($\varepsilon > 0.9$) is substantially influenced by temperature (Zhao et al. 2004b,c; Coquard et al. 2009, 2012). Given the temperature influence on effective conductivity, further experimental investigations were carried out to take account for ambient temperature variation on the effective conductivity of open-cell Al foams.

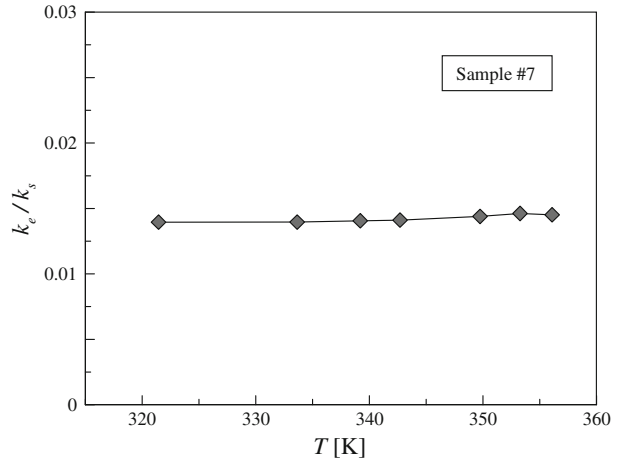
The effective thermal conductivity of an Al foam specimen saturated in air (marked as sample #7 in Table 1) was measured at different ambient temperatures. As depicted in Fig. 7, within the temperature range of 320–360 K considered, the variation of ambient temperature has little influence on the effective conductivity. As a result, with a fluctuation within 2 %, the effective conductivity of open-cell Al foams may be treated as temperature independent.

4.3 Effect of Pore Size (PPI)

Expressed conventionally in pores per inch (PPI), pore size is a fundamental morphology parameter for cellular foams. For convective and radiative heat transfer in open-cell metallic foams, it has been established that PPI affects significantly the thermal performance (Zhao et al. 2004a,b; Coquard et al. 2009). For heat conduction in high porosity open-cell Al foams, the experimental results on the influence of PPI upon effective thermal conductivity are analyzed below.

Figure 8a, b plots separately the experimentally measured effective conductivity as a function of pore size PPI from the present study and open literature (Calmidi and Mahajan

Fig. 7 Temperature independence of effective thermal conductivity of selected open-cell Al foam sample (#7 in Table 1) saturated in air ($\varepsilon = 0.957$, 8 PPI)



1999) for air- and water-saturated Al foams. Depending on porosity, the test data are divided into four different groups: as the test samples do not have exactly the same porosity, each group takes the average as the representative porosity. It is observed from the results of Fig. 8 that, for a give representative porosity, pore size variation in the range of 5–40 PPI has little influence upon the effective conductivity. For instance, with $\varepsilon \sim 0.910$, the effective conductivity data of air-saturated Al foams having different pore sizes (5, 7, 10 and 40 PPI) coincide on a curve of $k_e/k_s = 0.0282$. As a result, with the effects of convective and radiative heat transfer neglected, the influence of pore size on the effective conductivity may be safely neglected for high porosity open-cell Al foams.

4.4 Estimate of Node Size

High porosity open-cell Al foams typically consist of tetrakaidecahedron-like cells having 8 hexagonal and 6 square faces made of solid Al ligaments. Whilst regular nodes are present at the intersection of ligaments, occasionally lumps exist where the ligaments join (see Fig. 9). It needs to be clearly stated here that the lumps at the intersection of ligaments are easily misunderstood and treated as the nodes. The nodes, a little bigger than ligaments in thickness, are formed at the joints by metal ligaments, while the lumps with much bigger size exhibit square-like cross-sectional shape. During the direct foaming process (an alternative way to fabricate metallic foams), this may be caused by the foaming gas not easily expanded to overflow from the minimum exit of the tetrakaidecahedron cells, e.g., the square face in a single tetrakaidecahedron cell shown in Fig. 2. Upon solidification, the lumps are formed where the foaming gas is not entirely expanded and hence blocked. Compared with direct forming approach, precision casting as used to fabricate the Al foams used in the present study can avoid such defects in foams; see Fig. 1b.

For both the prediction of effective conductivity and the better understanding of thermal transport phenomena in open-cell metallic foams, an accurate description of node size is critical. The node sizes estimated by different analytical models are summarized in Table 2. As previously discussed, by adopting a hexagonal honeycomb shape to represent the topology of open-cell metallic foams, square and circular nodes having unrealistically large node sizes (node thickness to half of ligament thickness equal to 22.22 and 10.53) were reported by Calmidi and Mahajan (1999); Bhattacharya et al. (2002). Given the implausibility of node

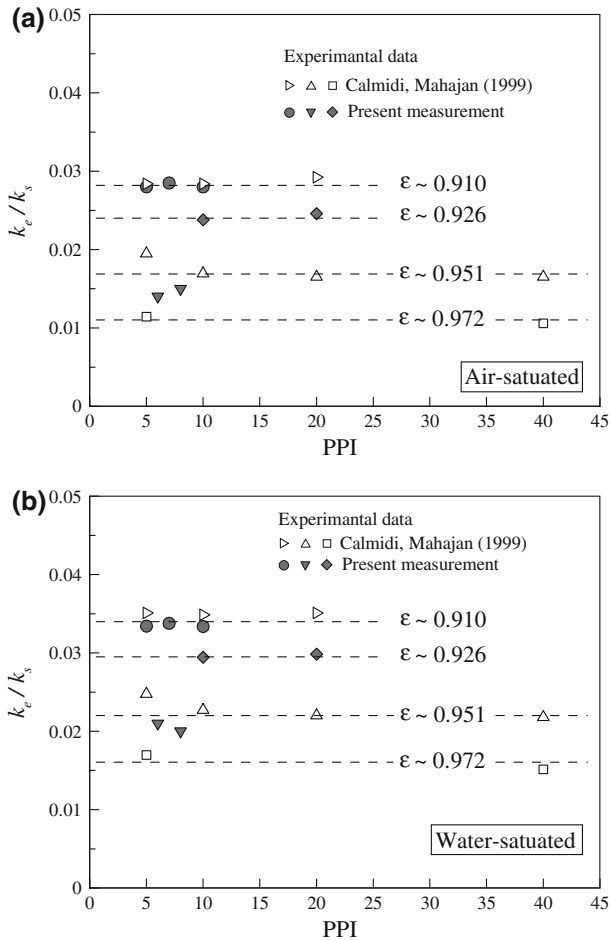


Fig. 8 Experimental results on pore size (PPI) effect upon effective thermal conductivity of high porosity open-cell Al foams saturated with: **a** air; **b** water

Fig. 9 Optical image of open-cell Al foam with lump at cell ligament joints (Bhattacharya et al. 2002; Calmidi and Mahajan 1999)

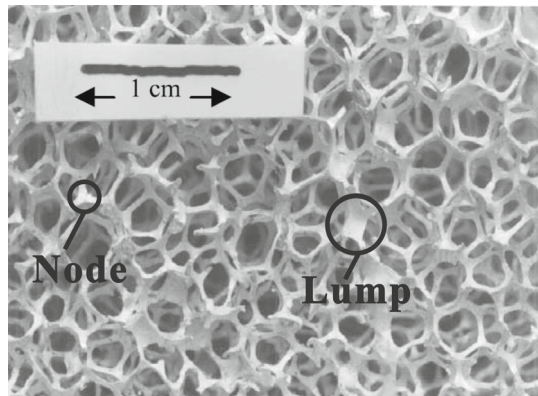


Table 2 Fundamental unit cell models specifically developed for open-cell foam like porous media

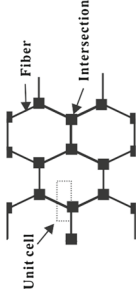
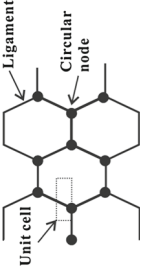
Model	Unit cell	Expression	Comments
Two-dimensional hexagonal unit cell with square node (Calmidi and Mahajan 1999)		$k_e = \left(\left(\frac{2}{\sqrt{3}} \right) \left(\frac{r \left(\frac{b}{L} \right)}{k_f + \left(1 + \frac{b}{L} \right) \frac{(k_s - k_f)}{3}} + \frac{(1-r) \left(\frac{b}{L} \right)}{k_f + \frac{2}{3} \left(\frac{b}{L} \right) (k_s - k_f)} \right) + \frac{\frac{\sqrt{3}}{2} - \frac{b}{4r}}{k_f + \frac{3\sqrt{3} \left(\frac{b}{L} \right) (k_s - k_f)}{4r}} \right)^{-1}$ <p>where $\frac{b}{L} = \frac{-r + \sqrt{r^2 + \frac{2}{\sqrt{3}}(1-\epsilon) \left(2-r \left(1 + \frac{4}{\sqrt{3}} \right) \right)}}{\frac{2}{3} \left(2-r \left(1 + \frac{4}{\sqrt{3}} \right) \right)}$ and $r = 0.09$</p>	<p>Unrealistic micro structure: hexagonal honeycomb shape with square nodes joined by the solid ligaments</p> <p>Valid in the porosity range $\epsilon < 1$ $e/d = t/a = 22.22$ Constant node size, unrealistically and extremely huge node</p>
Two-dimensional hexagonal unit cell with circular node (Bhattacharya et al. 2002)		$k_e = \left(\left(\frac{2}{\sqrt{3}} \right) \left(\frac{t/L}{k_f + \frac{1}{3} (k_s - k_f)} + \frac{\sqrt{3}(2-t/L)}{k_f} \right) \right)^{-1}$ <p>where $\frac{t}{L} = \frac{-\sqrt{3} - \sqrt{3 + (1-\epsilon) (\sqrt{3}-5)}}{1 + \frac{1}{\sqrt{3}} \frac{8}{3}}$ and $r = 0.19$</p>	<p>Two-dimensional semi-analytical model</p> <p>Unrealistic structure: hexagonal honeycomb shape with circular nodes joined by the solid ligaments</p> <p>Valid in the porosity range $\epsilon < 1$</p>

Table 2 continued

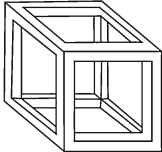
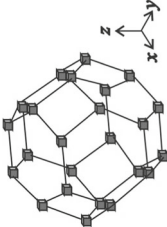
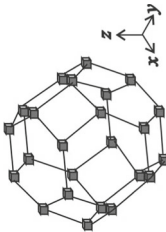
Model	Unit cell	Expression	Comments
Cubic cell (Paek et al. 2000)		$k_c = k_s t^2 + k_f (1 - t)^2 + \frac{2t(1-t)k_f k_s}{k_s(1-t) + k_f t}$ <p>where $t = \frac{1}{2} + \cos\left(\frac{1}{3} \cos^{-1}\left(\frac{4\pi}{3}\right) (2\varepsilon - 1)\right) + \frac{4\pi}{3}$</p>	<p>$e/d = t/a = 10.53$ Constant node size, unrealistically and extremely huge node Three-dimensional analytical model</p>
Tetradecahedron unit cell (Boomsma and Poulikakos 2001)		$k_c = \frac{\sqrt{2}}{2(R_A + R_B + R_C + R_D)}$ <p>where $R_A = \frac{4d}{(2e^2 + \pi d(1-e))k_s + (4 - 2e^2 - \pi d(1-e))k_f}$</p>	<p>Unrealistic micro structure: twelve cubic ligaments contained in a cube Valid in the porosity range $\varepsilon < 1$ Relatively good agreement with experimental data No node Three-dimensional semi-analytical model</p>
			<p>Realistic micro structure: tetradecahedron geometry with cubic nodes in intersection of ligaments Only valid in the porosity range $\varepsilon < 0.98$ Fairly good agreement with experimental data</p>

Table 2 continued

Model	Expression	Comments
Unit cell	$R_B = \frac{(e-2d)^2}{(e-2d)^2 k_s + (2e-4d - (e-2d)e^2) k_f}$ $R_C = \frac{(e-2d)^2}{(\sqrt{2}-2e)^2} k_f$ <p>where $R_D = \frac{2e}{e^2 k_s + (4-e^2) k_f}$</p> $d = \sqrt{\frac{\sqrt{2}(2-(5/8)e^3\sqrt{2}-2e)}{\pi(3-4e\sqrt{2}-e)}} \text{ and } e = 0.339$	<p>Geometrical and derivation mistakes</p> <p>$e/d = t/a < 2$ for $\varepsilon < 0.96$, shrunken node; $e/d = t/a > 2$ for $0.96 < \varepsilon < 0.98$, expanded node Variable node size with porosity, unrealistic node size and shape for $\varepsilon < 0.96$</p>
Tetradecahedron unit cell (Dai et al. 2010)		<p>Corrected and extended from the model of Boomsma and Poulikakos</p>
	<p>where $R_A = \frac{4d}{(2e^2 + \pi d(1-e)) k_s + (4-2e^2 - \pi d(1-e)) k_f}$</p> $R_B = \frac{(e-2d)^2}{(e-2d)^2 k_s + (2e-4d - (e-2d)e^2) k_f}$ $R_C = \frac{2(\sqrt{2}-2e)}{\sqrt{2}\pi d^2 k_s + 2(2-\sqrt{2}\pi d^2) k_f}$ <p>where $R_D = \frac{2e}{e^2 k_s + (4-e^2) k_f}$</p> $d = \sqrt{\frac{\sqrt{2}(2-(3/4)e^3\sqrt{2}-2e)}{\pi(3-2e\sqrt{2}-e)}} \text{ and } e = 0.189$	<p>Valid in the porosity range $\varepsilon < 1$</p> <p>Better agreement with experimental data</p> <p>$e/d = t/a < 2$ for $\varepsilon < 0.974$, shrunken node; $e/d = t/a > 2$ for $0.974 < \varepsilon < 1$, expanded node Variable node size with porosity, unrealistic node size and shape for, $\varepsilon < 0.974$</p>

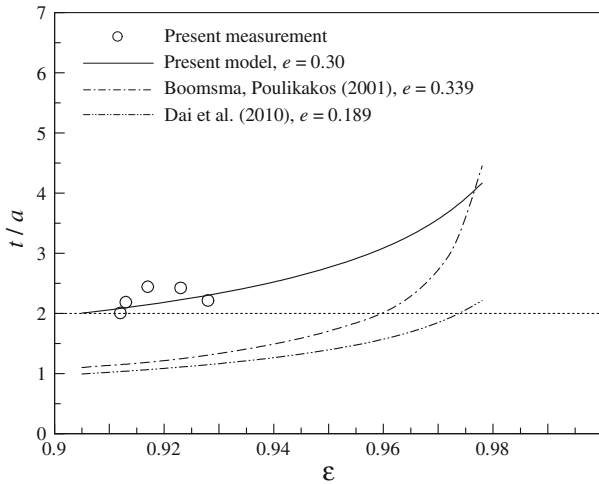


Fig. 10 Comparison of predicted node size from different models (Boomsma and Poulikakos 2001; Dai et al. 2010) and experimental measurement for high porosity open-cell Al foams

size estimation by models assuming 2D cell topologies, Boomsma and Poulikakos (2001) selected a more realistic 3D tetrakaidecahedron unit cell with cubic nodes to represent the foam structure. They assumed further that the size of the cubic nodes varies with foam porosity. However, Dai et al. (2010) pointed out that, whether the Boomsma–Poulikakos model is corrected or not, good agreement with experimental data as declared in their original paper, i.e., Figs. 2 and 3 of Boomsma and Poulikakos (2001), may not be achieved. Although Dai et al. (2010) attempted to correct and modify the original Boomsma–Poulikakos model, resulting in better agreement with experimental data, unrealistic prediction of node size seems to remain an issue.

Figure 10 compares the predictions of node size t/a by different models in the high porosity range. Boomsma and Poulikakos (2001) predict $t/a < 2$ at relatively low porosities ($0.90 < \epsilon < 0.96$) but $t/a > 2$ as the porosity is increased ($\epsilon > 0.96$). Given the structure of one-sixteenth of a single tetrakaidecahedron unit cell with cuboid nodes (Fig. 3), $t/a \geq 2$ must be satisfied to physically guarantee no shrinking exists at the ligament joints. In spite of the mistakes of the Boomsma–Poulikakos model, shrunken nodes are predicted within the porosity range of $0.90 < \epsilon < 0.96$. With the correction and modification of Dai et al. (2010), the situation becomes even worse for the porosity range within which shrunken nodes are found is extended to $\epsilon < 0.97$. In contrast, the present analytical model is devoid of faulty node size predictions, achieving expanded nodes whose size increases with increasing porosity for the full range considered ($0.90 < \epsilon < 1.0$). In comparison with the present measurements, the estimated node size by the model gives satisfactory agreement (Fig. 10).

4.5 Effect of Ligament Cross-sectional Areas and Shapes

4.5.1 Variable Cross-sectional Areas (Ligament Shape)

As discussed in Sect. 2.4, the solid cell ligaments look like dumbbells: relatively thick at both ends and thin in the middle (see Fig. 4). To quantify the influence of ligament cross-sectional areas (ligament shape) on the effective conductivity by using the present analytical model, a linear functional relationship for the cross-sectional area of the ligament is assumed.

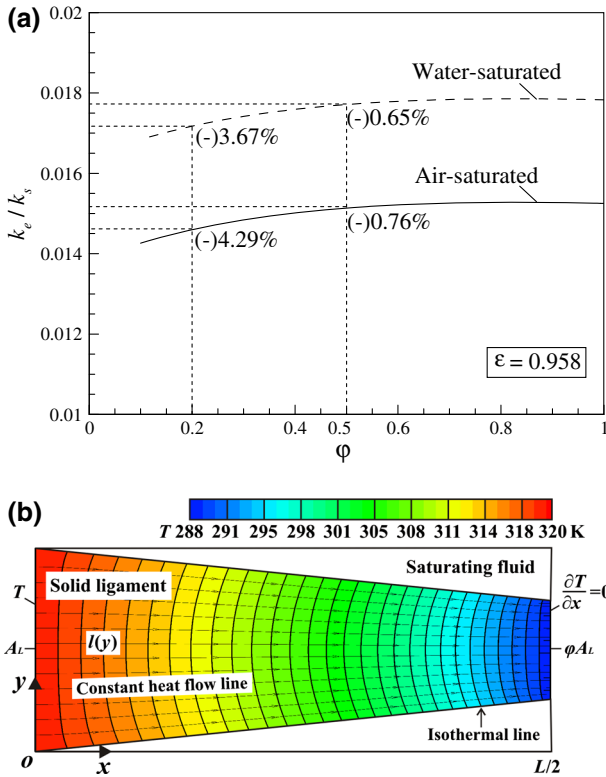


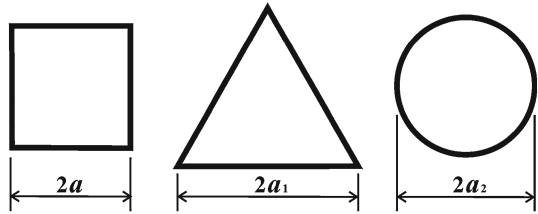
Fig. 11 Influence of variable ligament cross-sectional areas upon effective thermal conductivity: **a** analytical model prediction at porosity of 0.958; **b** distortion of local temperature field and constant heat-flow lines obtained from numerical simulations with constant wall temperature at $x = 0$ and symmetric boundary at $x = L/2$ for a single half ligament saturated in air ($\phi = 0.5$)

For a given porosity of 0.958, Fig. 11a plots the predicted effective conductivity k_e/k_s as a function of ligament cross-sectional area ratio ϕ . For both air- and water-saturated Al foams, the change in cross-sectional area ratio has little influence upon the effective conductivity. For instance, with ϕ decreased from 1.0 (uniform straight ligament) to 0.5 (half cross-sectional area in the middle), the effective conductivity is reduced only by 0.65 and 0.76 % for air and water as the saturating fluid, respectively. Further numerical simulations of a single ligament ($\phi = 0.5$) saturated in air are conducted to investigate the thermal transport characteristics of non-uniform ligaments. As shown in Fig. 11b, as the cross-sectional area along a single ligament is linearly reduced from its end toward the center, the numerical simulated constant temperature lines are distorted and hence the heat conduction distance is elongated, leading to increased thermal tortuosity. However, as the ligament cross-sectional area is only slightly varied ($\phi \sim 0.9$) for real open-cell Al foams (Fig. 1b), its influence on the effective conductivity of the foam may be neglected.

4.5.2 Variable Cross-sectional Shapes

As previously discussed, during the model derivation, ligaments having a square cross-section are assumed. Other cross-sectional shapes such as circle and triangle may also be assumed. However, it can be shown that there is no influence upon the effective thermal conductivity

Fig. 12 Illustration of ligament cross-sectional shapes: *square*, *equilateral triangle*, and *circle*



of metal foams for a given porosity and fixed pore size (ligament length, L). For a given relative density (or porosity) with maintaining the pore size, the cross-sectional area of ligaments remains unchanged regardless of the cross-section shapes, i.e., $A_{\text{square}} = A_{\text{triangle}} = A_{\text{circle}} = 4a^2$ (see Fig. 12). Here, the cross-sectional area for different shapes takes the form:

$$A_{\text{square}} = (2a)^2 \tag{20a}$$

$$A_{\text{triangle}} = \frac{\sqrt{3}}{4}(2a_1)^2 \tag{20b}$$

$$A_{\text{circle}} = \frac{\pi}{4}(2a_2)^2, \tag{20c}$$

where $a_1 \sim 1.519a$ and $a_2 \sim 1.128a$ for the same cross-section area as the square-shaped ligaments. It is therefore when dealing with metallic foams whose ligaments' cross-sectional shapes are triangle or circular, the corresponding ligament thickness a_1 or should be implemented into the determination of topological parameters. The surface area density of the ligaments having the three different cross-sectional shapes is changed although other parameters, e.g., porosity, pore size are fixed. However, the surface area does not contribute to the effective thermal conductivity as no heat transfer between the solid ligaments and surrounding fluid and radiation from the solid ligaments were assumed. On the other hand, the surface area will play a significant role in other heat transfer modes, e.g., radiation and forced convection, which are not included in the present study.

4.6 Contribution of Fluid Phase

High porosity open-cell metallic foams are widely as adopted to construct heat sinks for electronic cooling and compact heat exchangers (Lu et al. 1998; Mahjoob and Vafai 2008; Zhao et al. 2004a) where air is the working fluid. Given the large thermal conductivity ratio between the parent material and the saturating fluid (e.g., $k_s/k_f > 8000$ for air-saturated Al foams), the contribution of heat transported through the fluid phase can safely be neglected. This leads to a remarkably simple form of the dependence of k_e/k_s upon porosity, as expressed in Eq. (19). One wonders then when the contribution of fluid phase cannot be neglected. To this end, by using the present analytical model, Fig. 13 plots the effective thermal conductivity (k_e/k_s) as a function of the thermal conductivity ratio (k_s/k_f) for a given porosity of 0.958. It is observed that the effective conductivity is increased by about 10 % as the conductivity ratio is decreased from 8000 to 538. As the conductivity ratio is further decreased, the effective thermal conductivity of the fluid-saturated foam is dramatically increased due mainly to the contribution of fluid phase. As a result, if deviation within 10 % (at $k_s/k_f = 538$) for the estimate of effective conductivity may be tolerated, the contribution of fluid phase to effective conductivity may be neglected. The simple explicit expression of Eq. (19) may be

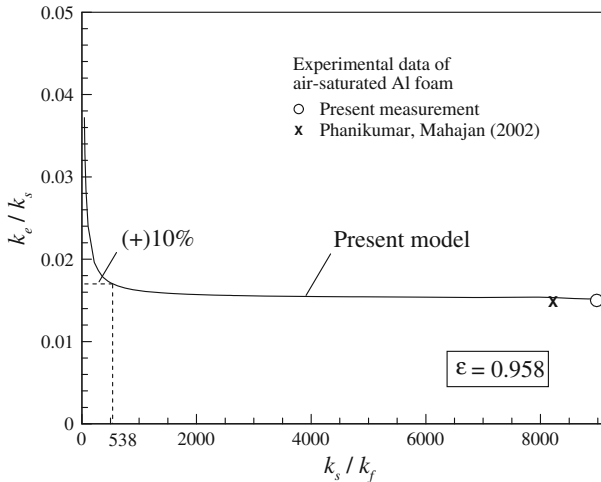


Fig. 13 Analytically predicted effective thermal conductivity of fluid-saturated metallic foams with open cells (porosity fixed at 0.958) plotted as a function of thermal conductivity ratio (k_s/k_f).

employed to calculate the effective thermal conductivity of high porosity open-cell metallic foams.

4.7 Interactive Heat Conduction Between Fluid and Ligaments

During the previous model derivation, heat transfer through the unit cell is assumed to be parallel separately via solid ligaments and the saturating fluid. The interactive heat conduction between the two phases (solid and fluid) is assumed to be neglected. However, there exists heat conduction between the two phases which will affect the overall effective thermal conductivity of the bulk porous media even if the natural convection and thermal radiation are both neglected. To quantitatively investigate the influence of interactive heat conduction upon the effective thermal conductivity of the bulk porous media, numerical simulation based on the finite volume method (FVM) embedded within commercially available software ANSYS-CFX 14.0 is employed. A solid geometry is generated using SOLIDWORKS™ the same as the CV depicted in Fig. 3 ($\varepsilon = 0.958$) and then exported to ANSYS-CFX 14.0 for steady-state heat conduction analysis. The numerically simulated results for different saturating fluid (different k_s/k_f ratios) are plotted against experimental data shown in Fig. 14. The effective thermal conductivity obtained by numerical simulation agrees quite well with the experimental results from the present measurements and the open literature (Phanikumar and Mahajan 2002), validating the numerical model. It is observed in Fig. 14 that the maximum deviation (decrease) in the effective conductivity (k_e/k_s) without interactive heat conduction is 8.66 % when a small thermal conductivity ratio (k_s/k_f) is 4.36. As the conductivity ratio is further increased, the deviation in the effective conductivity with/without interactive heat conduction is dramatically reduced, such as 1.96 % for water saturation and 0.10 % for air saturation (detailed results are tabulated in Table 3). Consequently, the present assumption of parallel heat conduction in the two phases is reasonable. Further, for fluid-saturated metallic foams with open cells, if deviation within 8.66 % (at $k_s/k_f = 4.36$) for the estimate of effective conductivity may be tolerated, the contribution of interactive heat conduction between the solid and fluid phase to effective conductivity may be neglected.

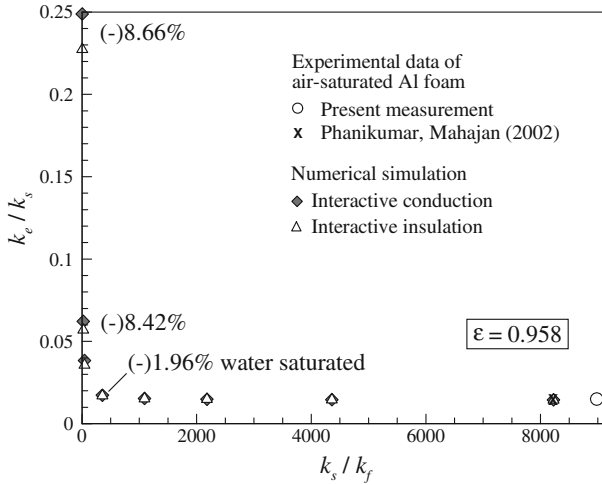


Fig. 14 Numerically simulated effective thermal conductivity of open-cell metallic foams saturated by various fluids (porosity fixed at 0.958): interactive conduction effect

Table 3 Deviation analysis of numerically simulated effective thermal conductivity for open-cell metallic foams saturated by various fluids for a given porosity ($\epsilon = 0.958$)

k_s/k_f	k_e/k_s			Saturated fluid
	Interactive conduction	Interactive insulation	Relative error (%)	
9688.9	0.014494	0.014481	0.086	Air
8226.4	0.014513	0.014498	0.101	
4360	0.014626	0.014598	0.190	
2180	0.014867	0.014811	0.374	
1090	0.015348	0.015237	0.724	
436	0.016792	0.016514	1.652	Water
355.6	0.017335	0.016996	1.960	
43.6	0.038371	0.035674	7.027	
21.8	0.062198	0.056963	8.417	
4.36	0.248838	0.227273	8.666	

5 Conclusions

A physically sound yet remarkably simple analytical model is developed for the effective thermal conductivity of metallic foams with open cells. With parallel heat conduction through solid cell ligaments and saturating fluid assumed (numerically validated), a realistic tetrakaidecahedron unit cell having cuboid nodes is selected to represent the cellular topology of high porosity open-cell Al foams fabricated via the precision casting route. The analytical model predictions are validated against experimental measurements, with good agreement achieved. It is demonstrate that the influence of pore size and ligament cross-sectional shape upon the effective thermal conductivity of the foam can be safely neglected. Compared with other existing models that predict unrealistically large nodes, the present model gives physically reasonable prediction of node size for open-cell metallic foams. When the thermal conductivity ratio of metallic ligaments to saturating fluid is over 538, the contribution of heat conduction via the fluid phase to the effective thermal conductivity may be neglected.

Further, for open-cell metallic foams saturated with typical engineering fluids such as air or water, the contribution of interactive heat conduction between the solid and fluid phase to the overall effective conductivity can be safely neglected.

Acknowledgments This work was supported by the National 111 Project of China (B06024), the National Basic Research Program of China (2011CB610305), and the National Natural Science Foundation of China (51206128).

Appendix

A cuboid-shaped control volume (CV) for one-sixteenth of a single tetrakaidecahedron unit cell with cuboid nodes having thickness t and cross-sectional area A_t is selected to represent the topology of open-cell foams, as shown in Fig. 3. The CV contains three ligaments with half cross-sectional area and four cuboid nodes: two have half cross-sectional area and the other two have one fourth cross-sectional area. Accordingly, the volumes of the three ligaments and four cuboid nodes may be calculated as:

$$V_L = \frac{A_L}{2}(L - t) \times 3 \tag{21}$$

$$V_t = \left(\frac{A_t}{4} \times \frac{t}{2} + \frac{A_t}{2} \times \frac{t}{2} \right) \times 2, \tag{22}$$

where A_t and A_L are the cross-sectional area of the node and ligament, t and L are the thickness and length of the node and ligament, respectively. The relative density ρ^* of the open-cell Al foam then becomes $\rho^* = (V_L + V_t)/V_{CV}$, where $V_{CV} = \sqrt{2}L^3$ is the volume of the cuboid-shaped CV. Finally, by introducing the two dimensionless parameters α and e defined in Eqs. (8a) and (9), the foam relative density ρ^* may be expressed as:

$$\rho^* = 1 - \varepsilon = \left[\frac{6(1 - e) + 3\alpha e}{4\sqrt{2}} \right] \times \frac{A_L}{L^2}, \tag{23}$$

where ε is the foam porosity. With reference to Fig. 3, the variation of heat transfer area integrated along the s -direction in the selected CV may be calculated as:

$$\int_0^{H(s)} \frac{1}{A_s} ds = \int_0^{H_1(s)} \frac{1}{A_{s1}} ds + \int_{H_1(s)}^{H_2(s)} \frac{1}{A_{s2}} ds + \int_{H_2(s)}^{H_3(s)} \frac{1}{A_{s3}} ds, \tag{24}$$

where the first and third items in Eq. (24) are separately the heat transfer path through the one fourth nodes and one eighth nodes, whilst the second term is that through the inclined ligaments (the horizontal ligament is insulated due to bilateral symmetry). For ligaments and nodes having constant cross-sectional areas, the area in each item of Eq. (24) is calculated as:

$$A_{s1} = 0.5A + 0.5A = A \tag{25a}$$

$$A_{s2} = 0.5A_L + 0.5A_L = A_L \tag{25b}$$

$$A_{s3} = 0.25A + 0.25A = 0.5A. \tag{25c}$$

Substitution of Eqs. (25a)–(25c) into Eq. (24) results in:

$$\int_0^{H(s)} \frac{1}{A_s} ds = \frac{0.5t}{A} + \frac{0.5t}{0.5A} + \frac{L-t}{A_L} = \left(1 - \beta + 1.5\frac{\beta}{\alpha}\right) \frac{L}{A_L}. \quad (26)$$

With the heat transfer area and height of the CV separately determined as $A_0 = 2L^2$ and $H_c = \sqrt{2}L/2$ (see Fig. 3), the heat transported through the solid ligaments and nodes may be obtained as:

$$\left(\frac{H_c}{A_0}\right) / \left(\int_0^{H(s)} \frac{1}{A_L(s)} ds\right) = \frac{\sqrt{2}}{4(1-e + \frac{3e}{2\alpha})} \times \frac{A_L}{L^2}. \quad (27)$$

Finally, substitution of Eqs. (23) and (27) into Eq. (7) yields an explicit expression for the effective thermal conductivity of open-cell metal foams, i.e., Eq. (11).

References

- Bhattacharya, A., Calmidi, V.V., Mahajan, R.: Thermophysical properties of high porosity metal foams. *Int. J. Heat Mass Transf.* **45**(5), 1017–1031 (2002)
- Boomsma, K., Poulikakos, D.: On the effective thermal conductivity of a three-dimensionally structured fluid-saturated metal foam. *Int. J. Heat Mass Transf.* **44**(4), 827–836 (2001)
- Calmidi, V.V., Mahajan, R.: The effective thermal conductivity of high porosity fibrous metal foams. *J. Heat Transf.* **121**(2), 466–471 (1999)
- Coleman, H.W., Steele, W.G.: *Experimentation, Validation, and Uncertainty Analysis for Engineers*. Wiley, Hoboken (2009)
- Coquard, R., Rochais, D., Baillis, D.: Experimental investigations of the coupled conductive and radiative heat transfer in metallic/ceramic foams. *Int. J. Heat Mass Transf.* **52**(21), 4907–4918 (2009)
- Coquard, R., Rousseau, B., Echegut, P., Baillis, D., Gomart, H., Iacona, E.: Investigations of the radiative properties of Al–NiP foams using tomographic images and stereoscopic micrographs. *Int. J. Heat Mass Transf.* **55**(5), 1606–1619 (2012)
- Dai, Z., Nawaz, K., Park, Y., Bock, J., Jacobi, A.: Correcting and extending the Boomsma–Poulikakos effective thermal conductivity model for three-dimensional, fluid-saturated metal foams. *Int. Commun. Heat Mass Transf.* **37**(6), 575–580 (2010)
- Haack, D.P., Butcher, K.R., Kim, T., Lu, T.J.: Novel lightweight metal foam heat exchangers. *Porvair Fuel Cells* (2001)
- Hsu, C., Cheng, P., Wong, K.: Modified Zehner–Schlunder models for stagnant thermal conductivity of porous media. *Int. J. Heat Mass Transf.* **37**(17), 2751–2759 (1994)
- Hunt, M., Tien, C.: Effects of thermal dispersion on forced convection in fibrous media. *Int. J. Heat Mass Transf.* **31**(2), 301–309 (1988)
- Incropera, F.P., Lavine, A.S., DeWitt, D.P.: *Fundamentals of Heat and Mass Transfer*. Wiley, Hoboken (2011)
- Kumar, A., Reddy, R.: Modeling of polymer electrolyte membrane fuel cell with metal foam in the flow-field of the bipolar/end plates. *J. Power Sources* **114**(1), 54–62 (2003)
- Landauer, R.: The electrical resistance of binary metallic mixtures. *J. Appl. Phys.* **23**(7), 779–784 (1952)
- Lu, T.J., Stone, H., Ashby, M.A.: Heat transfer in open-cell metal foams. *Acta Mater.* **46**(10), 3619–3635 (1998)
- Mahjoob, S., Vafai, K.: A synthesis of fluid and thermal transport models for metal foam heat exchangers. *Int. J. Heat Mass Transf.* **51**(15), 3701–3711 (2008)
- Maxwell, J.C.: *A Treatise on Electricity and Magnetism*, vol. 1. Clarendon Press, Oxford (1881)
- Ozmat, B., Leyda, B., Benson, B.: Thermal applications of open-cell metal foams. *Mater. Manuf. Process.* **19**(5), 839–862 (2004)
- Paek, J., Kang, B., Kim, S., Hyun, J.: Effective thermal conductivity and permeability of aluminum foam materials 1. *Int. J. Thermophys.* **21**(2), 453–464 (2000)
- Phanikumar, M., Mahajan, R.: Non-Darcy natural convection in high porosity metal foams. *Int. J. Heat Mass Transf.* **45**(18), 3781–3793 (2002)

- [Progelhof, R., Throne, J., Ruetsch, R.: Methods for predicting the thermal conductivity of composite systems: a review. *Polym. Eng. Sci.* **16**\(9\), 615–625 \(1976\)](#)
- [Russell, H.: Principles of heat flow in porous insulators. *J. Am. Ceram. Soc.* **18**\(1–12\), 1–5 \(1935\)](#)
- [Tadrist, L., Miscevic, M., Rahli, O., Topin, F.: About the use of fibrous materials in compact heat exchangers. *Exp. Therm. Fluid Sci.* **28**\(2\), 193–199 \(2004\)](#)
- [Tawfik, H., Hung, Y., Mahajan, D.: Metal bipolar plates for PEM fuel cell—a review. *J. Power Sources* **163**\(2\), 755–767 \(2007\)](#)
- [Thompson, D.W.: On growth and form. On growth and form \(1942\)](#)
- [Thomson, W.S.: On the division of space with minimum partitional area. *Acta Math.* **11**\(1–4\), 121–134 \(1887\)](#)
- [Tsotsas, E., Martin, H.: Thermal conductivity of packed beds: a review. *Chem. Eng. Process.* **22**\(1\), 19–37 \(1987\)](#)
- [Weaire, D.L., Hutzler, S.: *The Physics of Foams*. Oxford University Press, Oxford \(1999\)](#)
- [Yang, X.H., Lu, T.J., Kim, T.: Thermal stretching in two-phase porous media: physical basis for Maxwell model. *Theor. Appl. Mech. Lett.* **3**\(2\), 021011–021015 \(2013\)](#)
- [Zhao, C.Y., Kim, T., Lu, T.J., Hodson, H.: Thermal transport in high porosity cellular metal foams. *J. Thermophys. Heat Transf.* **18**\(3\), 309–317 \(2004a\)](#)
- [Zhao, C.Y., Lu, T.J., Hodson, H.: Thermal radiation in ultralight metal foams with open cells. *Int. J. Heat Mass Transf.* **47**\(14\), 2927–2939 \(2004b\)](#)
- [Zhao, C.Y., Lu, T.J., Hodson, H., Jackson, J.: The temperature dependence of effective thermal conductivity of open-celled steel alloy foams. *Mater. Sci. Eng. A* **367**\(1\), 123–131 \(2004c\)](#)